SERS detection and DFT calculation of 2-naphthalene thiol adsorbed on Ag and Au probes

Nisha Rani Agarwal [a,1], Andrea Lucotti [a], Matteo Tommasini [a], Fortunato Neri [b], Sebastiano Trusso [c,*], Paolo Maria Ossi [d]

[a] Dipartimento di Chimica, Materiali e Ingegneria Chimica, Politecnico di Milano, Piazza Leonardo da Vinci 32, Milano 20133, Italy
[b] Dipartimento di Fisica e di Scienze della Terra, Università di Messina, V.le Ferdinando Stagno d'Alcontres 31, 98166, Messina, Italy
[c] CNR-IPCF, Istituto per i Processi Chimico-Fisici, V.le Ferdinando Stagno d'Alcontres 37, 98158, Messina, Italy
[d] Dipartimento di Energia and Centre for NanoEngineered Materials and Surfaces, NEMAS, Politecnico di Milano, Via Ponzio 34-3, 20133, Milano, Italy

A B S T R A C T

Two different surface enhanced Raman scattering (SERS) sensors are described, tested and compared against the detection of 2-naphthalenethiol (2NPT, a volatile compound) in both solution state as well as vapor phase. The first sensor is based on an optical fiber properly modeled to induce the adhesion of colloidal Ag nanoparticles on its surface. Excitation and detection of the Raman signal is performed through the optical fiber that can be used as in situ probe for the detection of molecules adsorbed on the SERS sensitized surface. The second SERS sensor is based on nanostructured substrates consisting of Au nanoparticles produced by pulsed laser deposition in presence of a controlled Ar atmosphere. Details at the nanometer scale were observed by SEM and TEM imaging to understand the size and structure of the islands formed as a function of deposition parameters that were selected in order to maximize their SERS response. The sensitivity of the substrates to volatile species was tested by letting evaporate controlled drops of a methanol solution of 2NPT in a chamber of known volume, where the substrate was placed. After complete evaporation of the drops, this provided an in-situ environment suitable for vapor phase measurements at known concentration. SERS spectra were collected after exposing the substrates to the environment within the chamber (vapor phase measurements) or dipping them in a solution for condensed state measurements. The complete absence of the SH stretching peak in the SERS spectra proves the covalent bonding of 2NPT to the metal substrates via the sulfur atom. DFT calculations, including metal-sulfur interaction, provide a good description of the observed SERS spectra. The reported data allow concluding that our SERS substrates are suitable for detection of volatile compounds.

a r t i c l e i n f o
Article history:
Received 1 February 2016
Received in revised form 23 June 2016
Accepted 24 June 2016
Available online 25 June 2016

Keywords:
Volatile thiols
SERS sensors Fiberoptic
Pulsed laser deposition
Chemical kinetics

1. Introduction

The literature shows an increasing interest in developing plasmonic substrates with controlled nanostructure for advanced spectroscopic applications. Tuning plasmonic resonance allows optimization of the surface enhanced spectroscopic response of chemical species adsorbed on the substrate, thus allowing their sensing through the detection of the associated molecular spectra, even at low concentrations. Among available spectroscopies, SERS (Surface Enhanced Raman Spectroscopy) is able to detect low concentration of an analyte [1,2]. Volatile chemicals of environmental interest are found in air at low concentrations and hence are good candidates for SERS detection. For instance, it has been recently demonstrated that suitably functionalized gold substrates show a SERS signal sensitive to environmental volatile organic compounds, thus allowing their sensing even though it may be indirect [3].

In this contribution, we focus on the development of nanostructured substrates for direct SERS analysis of volatile sulfur-containing species, focusing on thiols. Thiols are known to interact covalently with noble metal surfaces, establishing a sulfur-metal bond that has been also exploited for producing self-assembled monolayers on flat gold surfaces [4]. Similar to thiols, sulfur-silver interaction has been reported in the formation of stable silver-thiophene nanocomposites [5] and SERS response of thiophene-2-carboxylic acid has been reported [6]. Hence, we

Abbreviations: SERS, surface enhanced Raman scattering; 2NPT, 2-naphthalenethiol; PLD, pulsed laser deposition; DFT, density functional theory.

* Corresponding author. E-mail address: trusso@me.cnr.it (S. Trusso).

[1] Present address: Department of biology and biological engineering, Chalmers University of technology, Kemivägen 9, 412 96 Gothenburg, Sweden.

Published Journal Article available at: http://dx.doi.org/10.1016/j.snb.2016.06.143

expect that organic sulfur species like thiols or thiophenes would generally provide SERS signals. Aromatic thiols, thiophenes and polycyclic aromatic sulfur heterocycles are expected sources of sulfur in fossil fuels [7]. Chromatography shows the presence of thiophenic polycyclic aromatic sulfur heterocyclics in crude oils and coal [8,9] as well as in petroleum condensate and volatile oils [10]. Sensitive analytical methods such as SERS, which also provide information on chemical structure, are interesting additional tools for the investigation of the complex molecular composition of fossil fuels [11,12].

We report here, the development and use of two different plasmonic substrates suitable for detection of 2-naphthalene-thiol (2NPT) through SERS. 2NPT was chosen as a representative thiol of geochemical interest, difficult to detect with GC/MS methods [7], for which the investigation of the SERS signal in solution state was reported [13].

The first SERS device is a fiber-optics with optimized geometry at the tip [14] covered by silver nanoparticles immobilized on the outer surface of the fiber. The second SERS probe is constituted by a nanostructured film obtained by controlled pulsed laser deposition (PLD) of gold on silicon and Corning glass [15]. While SERS is usually employed on solution state samples [16,17], in this contribution we show that it is possible to use SERS to detect volatile species as well. This is particularly appealing for environmental or industrial sensing of air pollutants. In fact, a SERS dosimeter could be easily deployed and analyzed at later times in the laboratory (provided that the analyte chemisorbs on the substrate). On the other hand, SERS fiber optics could be used for remote on-line sensing.

Cited literature suggests that attempts are being made to differentiate between different kinds of thiols while they are being extracted from petroleum; this makes a properly designed SERS substrate a promising complementary analytical tool for this kind of application. Finally, the analysis of the DFT models presented in this work (including metal-sulfur interaction) provides the compared assignment of the main Raman/SERS signals of 2NPT.

2. Materials and methods

2.1. Preparation of the SERS active fiber-optic tip

A silica fiber was chosen for SERS measurements with an inner core diameter of 200 μm and a numerical aperture of 0.22. The protective layer of the silica fiber was removed at one end of the fiber. A fine scratch was made normal to the axis of the fiber and was snapped in order to obtain a termination normal to the fiber optic axis, thus ensuring minimal optical losses when injecting laser light into the fiber core. The protective layer of the silica fiber was removed also from the other end of the fiber, which was successively cleaned with acetone and then subjected to a double static etching process to obtain a tip which has been later subjected to Lee-Meisel [18] Ag nanoparticle functionalization (immobilizing Ag-NP on silica through 3-aminopropyltrimethoxysilane). The detailed procedure for the fabrication of the whole fiber-optic double-tapered SERS sensor is given in [19,20].

2.2. Production of nanostructured Au substrates

Gold nanostructured substrates were produced using Pulsed Laser Deposition (PLD) technique. A KrF excimer laser (λ = 248 nm, pulse width 25 ns, repetition rate 10 Hz) was used for the deposition. The laser was focused on the target surface by a quartz lens and pure gold targets were placed on a rotating holder in order to avoid surface damage. The substrate used was 5049 Corning glass slides, which were positioned at a distance of 35 mm from the target. The PLD chamber was kept at a constant pressure of 70 Pa of Argon. The deposition of Au nanoparticles was fixed at 10000 laser shots and 2 J cm^{-2} of laser fluence. The characterization of these substrates were carried out by SEM and TEM imaging (respectively) using a Zeiss Supra 40 field ion microscope and a Zeiss Leo 912AB microscope operated at a voltage of 80 kV. The enhancement factor (EF) was evaluated by comparing the SERS intensity of methylene blue dye adsorbed on the nanostructured substrate with the normal Raman signal acquired on a gold flat surface. The two substrates were soaked into a 10^{-5} M concentrated aqueous solution for 1 h. Measurements were performed under identical experimental conditions: excitation wavelength source, integration time and microscope objective. A neutral density filter with optical density of 4 was needed to acquire the SERS spectrum to avoid saturation of the photo-detector, a proper normalization was performed to account for this filter. The estimated EF achieved was of the order of 10^4.

2.3. Reagents

$AgNO_3$ (99.8%), 3-aminopropyltrimethoxysilane (97%), HF (40%), trisodium citrate (99%), 2NPT (99%), were purchased from Aldrich chemicals and used without further purification. Methanol (99%), toluene (99%) and H_2O_2 (30%) were supplied by Fluka. Ethanol (99.9%), Xylene (98.5%) and H_2SO_4 (95–97%) were supplied by J.T. Baker.

2.4. Experimental setup for fiber optic SERS sensor

Controlled ethanol solutions of 2NPT were prepared and selected volumes of solution (of the order of 0.1 mL) were left to dry in a 3 L glass chamber which was sealed immediately after placing the solution drops. 2NPT is a solid that sublimates at ambient conditions. At 25 °C its vapor pressure is 0.00467 mmHg. In our setup 2NPT behaves as a vapor sublimating from solid state (*i.e.*, the precipitate left upon drying of the ethanol solution droplet loaded in the chamber). Since the left over 2NPT precipitate completely sublimates (we observe its disappearance), this ensures reaching a known concentration of 2NPT vapors in the given volume. Furthermore, since at ambient conditions the solid has a characteristic displeasing odor, it is certain that a vapor of NPT molecules effectively develops from the solid. This ensured reaching a known concentration of 2NPT vapors in the given volume. Depending on the chosen concentration of 2NPT ethanol solution, this procedure allowed reaching an approximate concentration of 10 ppb and 0.1 ppb in the chamber (1 ppb = 10^{-9} molar ratio). The molar ratio expresses the number of 2NPT moles over the number of moles of the air (plus the 2NPT ones) contained in the chamber. For simplicity we assumed ideal gas behavior, which implies that the molar concentration of 2NPT in air is given by the molar ratio divided by the standard molar gas volume of 22.4 L/mol. This gives [2NPT] = 4.4×10^{-11} mol/L. *In-situ* measurement is possible with the fiber optic since the SERS active tip can be sealed within the chamber and senses its environment. Hence time-dependent Raman measurements can be carried out while keeping sealed the chamber. This allows investigating the chemical kinetics of the substrate and represents a practical advantage of the fiber optic sensor.

Raman spectra have been recorded with HORIBA Jobin Yvon Labram HR800 equipped with Peltier cooled CCD detector and solid-state laser (Laser XTRA, Toptica Photonics) providing a 785 nm excitation wavelength. An Olympus BX41 microscope was used with a 10 x objective. An adaptive fiber-optic holder was built, in order to suitably couple the laser radiation with the fiber core. A sketch of the experimental apparatus is shown in Fig. 1a. The SERS measurements were carried out in an *optrode* configuration, where the same optical fiber (terminated with the SERS active layer) injects the laser excitation and collects the scattered

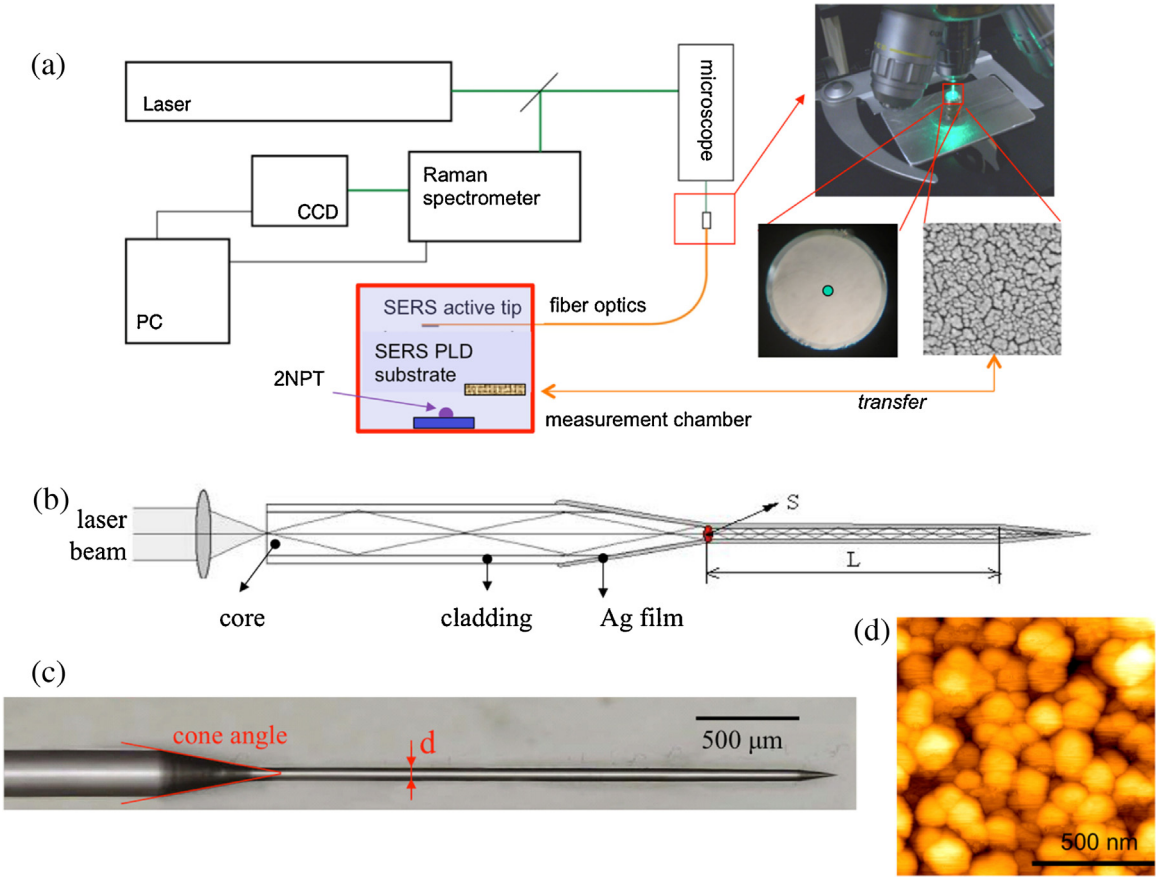

Fig. 1. (a) Sketch of the experimental setup of the fiber-optic SERS probe and the nanostructured Au substrate in the measurement chamber. The fiber-optic remains within the chamber while the Au nanostructured substrate is taken out of the chamber to perform Raman measurements, (b) Schematic of the light path traversed in the fiber-optic SERS probe layered by Ag nanoparticles. The length and the cross-sectional area of the etched part of the fiber-optic is $L \approx 3$ mm and $S \approx 2.5 \times 10^3$ μm^2 respectively, (c) Optical microscope image of a fiber-optic SERS probe, d = 50 mm, (d) AFM image of colloidal Ag nanoparticles immobilized on glass (see text for details for deposition procedure).

radiation (see Fig. 1b). We present the bright-field image of the fiber-optic in Fig. 1c. From Fig. 1d, AFM image of the colloidal Ag NPs immobilized on glass, the average diameter of the NP aggregates was found to be 110 ± 25 nm. Atomic Force Microscopy (AFM) measurements on nanostructured Ag films (Fig. 1d) were carried out with a Thermo Microscope (CT Research).

2.5. Experimental setup for the PLD Au substrates

The Au substrate was placed in the same chamber mentioned above with a maintained concentration of 2NPT. In-situ measurements are not possible with these substrates since the substrates have to be taken out of the sealed chamber and transferred under the microscope for SERS measurements as shown in Fig. 1a. Raman measurements were carried out with the same Raman equipment and 785 nm laser excitation line with a 50 x objective.

2.6. Density functional theory (DFT) calculations

We have simulated the off-resonance Raman response of 2NPT in order to compare it with experimental results and guide the peak assignment. Furthermore, two minimal molecular models (named 2NPT-Ag, 2NPT-Au with Ag or Au replacing the hydrogen atom in the −SH group) have been considered for the sake of analyzing the changes of the SERS signal compared to Raman. Calculations have been carried out at the B3LYP/cc-pVTZ level of theory; to describe Au and Ag atoms we have used Stuttgart effective core potentials (ECP28MDF for Ag and ECP60MDF for Au, both complemented with cc-pVTZ-PP basis set – see Refs. [21,22]).

The Gaussian09 rev. A.02 computer program [23] has been used to carry out the calculations; a set of custom in-house developed computer codes have been employed to simulate Raman spectra and analyze the nuclear displacements (see Supplementary Information).

3. Results and discussion

3.1. DFT-based peak assignment

Before addressing the experimental results on Raman/SERS spectra of 2NPT, it is worth to briefly review with the help of DFT calculations and literature data [15] the assignment of the most important Raman signals of 2NPT. The present assignments substantially match previous work [15] and make it more complete since we also consider DFT models for the adsorbate which are implied in our SERS experiments. We offer a more detailed description of the vibrational normal modes associated to the more relevant Raman/SERS features in the CH stretching ($\approx$3000 cm^{-1}) and fingerprint region (1800–300 cm^{-1}). We briefly summarize here the main results obtained in the description of the normal modes. Further details can be found in SI.

As Fig. 2 clearly shows that the overall trend of the Raman/SERS spectra is well reproduced by calculations which show that the intensity ratios, especially in the low frequency region, are affected by noble metal substitution. On the other hand Ag or Au substitutions have practically the same effect on the simulated spectra compared to 2NPT. This is in line with experimental observation,

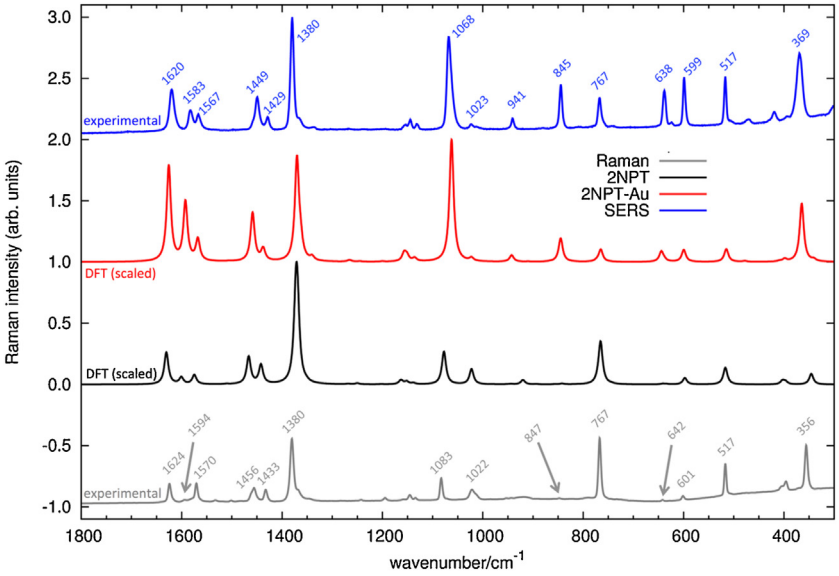

Fig. 2. Comparison of experimental Raman and SERS (on PLD Au substrates) signals of 2NPT with results from DFT calculations. Values of experimental wavenumbers are provided for selected lines. Wavenumbers of the simulated spectra from DFT calculations have been scaled by 0.98 (see also Table 1).

which show only minor differences in SERS of 2NPT promoted by Ag or Au nanostructures.

Five spectral regions can be identified (unscaled wavenumber from DFT are used to identify the modes, unless otherwise stated we refer to the 2NPT model – see also Table 1 for a synopsis of the main Raman lines in the fingerprint region, *i.e.*, below 1800 cm^{-1}):

i **CH stretching**. The main signal (3190 cm^{-1}) is due to the in-phase CH stretching of the four hydrogens located in the ring not carrying the sulfur atom. Its location is rather independent of (H, Ag, Au) substitution.

ii **Ring stretching**. Three signals (1664, 1633, 1607 cm^{-1}) are found whose nuclear displacement patterns can be associated to the G-line of other polycyclic aromatic compounds (see [24]). Compared to normal Raman, these modes are rather sensitive upon (Ag, Au) substitution (see Fig. 3) and their off-resonance Raman response is enhanced by about a factor of 10 compared to 2NPT. The observed changes of the spectral pattern between Raman and SERS are rather well accounted for by DFT calculations when comparing for instance 2NPT with 2NPT-Au (see Fig. 2). However, as evident from Fig. 3, the difference between Ag- *vs*. Au-substitution in the simulated DFT Raman spectra is limited.

iii **CS stretching/In-plane CH-bending/D-mode**. This comprises of three signals in 2NPT (1496, 1471, and the unresolved doublet 1400, 1397 cm^{-1}). The displacements more closely relate to the D-line pattern of PAHs belonging to the stronger almost degenerate modes found at 1400 and 1397 cm^{-1} (see also [24]). In 2NPT-Ag/2NPT-Au the D-mode is unique and it is delocalized over both condensed rings (1397, 1398 cm^{-1}, respectively). The other signals (with lower Raman intensity) can be described as collective in-plane CH bending coupled with collective CC stretching (see SI). Notably the higher wavenumber mode in this region (1496 cm^{-1}) is also associated to CS stretching, and it is red-shifted upon noble-metal substitution.

iv **CS stretching/ring-breathing**. The mode of 2NPT at 1099 cm^{-1} (and, to a less extent, 1043 cm^{-1}) is described as CS stretching coupled with ring breathing localized at the ring bearing the CS group (or at the other ring, for 1043 cm^{-1} mode). The lower wavenumber mode at 939 cm^{-1} is also characterized by CS stretching coupled with SH bending. As expected because of the contribution from CS and SH, the positions of the modes in this region are all affected by noble metal substitution. Notably, the stronger peak (ring breathing) gets red-shifted and enhanced by a factor of almost 20.

v **Collective skeletal bending/breathing**. Several resolved peaks are found in this region, all collectively involving several degrees of freedom and difficult to be described with a single character. One notable exception is the breathing of the aromatic core, which is found at 781 cm^{-1} and is barely affected by noble metal substitution both in wavenumber and Raman intensity. Another interesting very weak Raman mode is found at 648 cm^{-1} in 2NPT and is associated to collective CH out-of-plane bending. Interestingly its intensity is strongly enhanced (more than x20) upon noble metal substitution. This parallels experimental observation and the comparison between Raman and SERS in this region. The 642 cm^{-1} mode (expt.) is barely seen in Raman but becomes well resolved in SERS (638 cm^{-1}). We finally mention the C-X stretching modes at 362 cm^{-1} (X = Ag) and 372 cm^{-1} (X = Au). They are coupled with CS stretching and, compared with the corresponding mode of 2NPT at 353 cm^{-1} their intensity is markedly enhanced (more than x20), as expected for vibrations directly involving the metal-carbon bond.

3.2. *SERS behavior of the fiber optic sensor*

Before employing the fiber-optic SERS sensor, a reference (background) Raman spectra of the bare fiber optic sensor was recorded with 785 nm excitation (see Fig. 4) in the 100–3500 cm^{-1} spectral region.

As it is evident in Fig. 4a, the broad and strong Raman signals from the fiber optic in the low-frequency region (100–600 cm^{-1}) hinder the possibility to detect weak signals of the analyte in this spectral window. The inset of Fig. 4a shows the fiber optic background Raman signal zoomed in the 900–1800 cm^{-1} interval. Two broad bands are recorded at 1055 and 1183 cm^{-1}, which constitute the main background features in our fiber-optic SERS experiments. In Fig. 4b, the main peaks of the SERS spectrum of 2NPT collected with the fiber optic have been indicated. For this measurement, the chamber was prepared with an approximate concentration of 10 ppb of 2NPT. SERS spectra were then recorded through the fiber-optic sensor after about 15 min since the sealing of the measurement chamber. Within this time we observed the complete

Table 1
Comparison of experimental Raman and SERS (on PLD Au substrates) signals of 2NPT with results from DFT calculations.

Raman (exp) in cm^{-1}	0.98 scaled Raman (DFT)	unscaled Raman (DFT)	SERS (exp) in cm^{-1}	0.98 scaled 2NPT-Au (DFT)	unscaled 2NPT-Au (DFT)
1624	1631	1664	1620	1626	1659
1594	1600	1633	1583	1593	1625
1570	1575	1607	1567	1568	1600
1456	1466	1496	1449	1458	1488
1433	1442	1471	1429	1438	1467
1380	1372,1369	1400,1397	1380	1369	1397
1083	1077	1099	1066	1062	1084
≈919, broad	920	919	941	943	962
847	842	859 (weak)	845	845	862
767	765	781	767	765	781
642	635	648	638	644	657
601	598	610	599	600	612
517	516	527	517	515	525
356	346	353	369	365	372

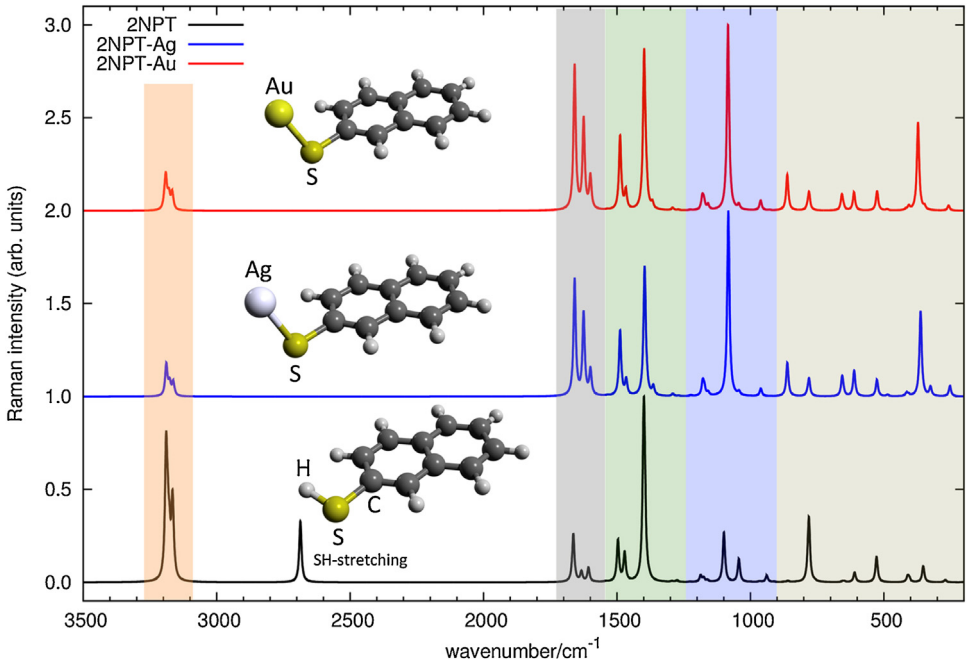

Fig. 3. Simulated Raman spectra of 2NPT and of the two models functionalized with Ag and Au used to help the interpretation of SERS of 2NPT (see text for details).

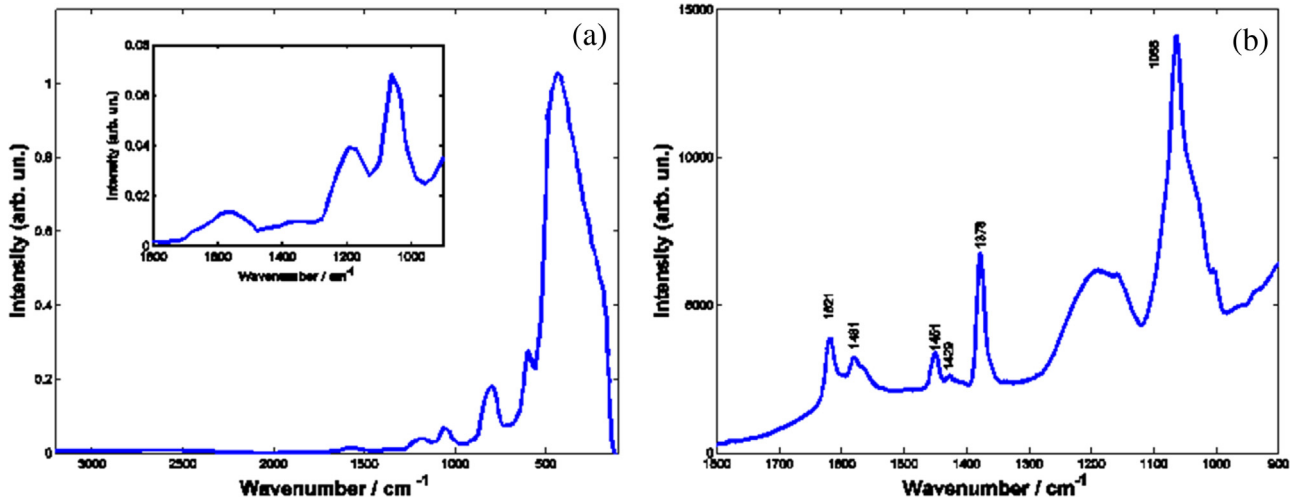

Fig. 4. (a) Reference Raman spectrum of the optical fiber in the 100–3500 cm^{-1} spectral region and in the 900–1800 cm^{-1} spectral region in the inset (excitation line: 514 nm). (B) Representative SERS spectrum of 2NPT (10 ppb) collected with the fiber optic sensor embedded in a 3 dm^3 chamber. The spectra were recorded 15 min after the introduction of the sensor in the chamber and with the 785 nm excitation line.

evaporation of the sample droplets containing 2NPT (see Experimental section for details).

We compare in Fig. 5, the FT-Raman and fiber-optic SERS spectra of 2NPT (the latter recorded with 785 nm excitation). It is evident from the *complete* disappearance of the SH stretching Raman line (2567 cm^{-1}) (marked with an arrow in Fig. 5) in the SERS that the molecule bonded to the silver colloid, replacing the S-H bond with an S-Ag bond at the nanostructured silver substrate. It is also noticeable that the most intense bands (1575, 1021, 999 cm^{-1}) in the SERS have been slightly red-shifted with respect to the corresponding Raman modes (1583, 1025, 1000 cm^{-1}). There has also been an effective change of the internal intensity ratios of the peaks. These observations are consistent with the results of DFT calculations on model molecules (see above). We can notice strong peaks at 1621, 1581, 1451, 1430, 1379, 1066 cm^{-1}, all assigned to the 2NPT moiety (see Figs. 4 b, 5 and SI). The 1621 and 1581 cm^{-1} lines are assigned to the characteristic CC stretching modes of the aromatic ring (ring stretching, see above). The 1451, 1430 and 1379 cm^{-1} peaks are assigned to in-plane CH bending coupled with ring CC stretching and CS stretching (1451, 1430 cm^{-1}) and to the D-mode (1379 cm^{-1}) of the two aromatic rings. The 1066 cm^{-1} peak is assigned to ring breathing coupled with CS stretching and in-plane CH bending.

3.3. Time dependent behavior of the fiber-optic SERS sensor

We have also tested the time dependent adsorption of 2NPT on the fiber-optic sensor using a concentration of approximately 0.1 ppb of the analyte in the chamber, as reported in the experimental section. We started to record SERS spectra 0, 10, 20, 30, 90 and 120 min after the complete evaporation of ethanol and sublimation of 2NPT. The recorded spectra are shown in Fig. 6.

The increase of Raman 2NPT features above the fiber optic Raman background spectrum is clearly visible as a function of time. To determine the time dependent behavior of the 1621 and 1378 cm^{-1} SERS signals (see Fig. 6), we have assessed their baseline corrected intensities as functions of time, measured after the complete sublimation of 2NPT on the bottom of the chamber.

As shown in Fig. 7, for both the 1621 and the 1378 cm^{-1} line, an initial exponential increase of the signal is observed, until at longer times a saturation value is reached, suggesting that the number of 2NPT molecules attached to the silver nanoparticles on the fiber optic progressively increases up to a limit where all SERS active sites are occupied.

The adsorption of molecules on a metallic surface is well described by the Elovich adsorption model [25]:

$$\frac{dq(t)}{dt} = ae^{-\alpha q(t)} \quad (1)$$

where $q(t)$ is the amount of adsorbed molecules at time t, and a and α are constants which depend on the system under study. Integrating Eq. (1) between t_0 and t, with $q(t_0)=0$, the amount of adsorbed molecules onto the surface at the time t is:

$$q(t) = \frac{\ln 10}{\alpha}\log\left[1 + a\alpha(t - t_0)\right] \quad (2)$$

The characteristic adsorption rate constant τ is given by $(a\alpha)^{-1}$. The results of the fitting procedure are shown in Fig. 7.

The characteristic time constants $(a\alpha)^{-1}$ as obtained from the fitting procedure are equal to 450 ± 100 s and 524 ± 120 s for the kinetic observed at 1621 cm^{-1} and 1378 cm^{-1} respectively.

3.4. SERS behavior of the PLD Au substrates

In Fig. 8(a) and (b) is shown the SEM and TEM images of the sample surface. As it can be seen the sample surface consists of nearly percolated structure made of gold islands with smooth edges. In previous works, we have characterized in detail the nanostructure formation mechanisms as a function of the adopted PLD deposition parameters. The first step consists of nanocluster condensation in the gas phase when the laser generated plasma expands in ambient atmosphere. In fact, collisions between the expanding plasma and the gas species lead to *in flight* formation of the nanoparticles. The dimension of these nanoclusters depends on the plasma mass density and energy (determined by the laser pulse spot area and energy), and on the gas density and atomic mass [26,27]). The second step takes place on the substrate surface. As soon as the nanoparticles land on the surface, they give rise to varied surface morphologies, depending on the laser pulse number adopted in the deposition process. At low laser pulse number, the surface morphology consists of a population of spherical isolated nanoparticles. At increasing numbers of laser pulses, the nanoparticles start to coalesce giving rise to aggregates, islands with round and smooth edges and percolated structures. The optical properties strongly depend on the final morphology of the sample and hence varied SERS enhancements. The SPR absorption peak position and shape is, in fact, strongly dependent on the size, shape and the spatial distribution of the nanostructure on the substrate surface. In general, a red-shift and a broadening of the SPR is observed when going from surface morphologies consisting of isolated nanoparticle towards percolated structures. The samples used in this work show a morphology characterized by the presence of gold islands separated by small gaps that can play a major role in the thin film SERS activity, acting as '*hot spots*' [28,29]. The SPR peak position lies between 700–730 nm and full width at half maximum (FWHM) of approximately 300 nm, so that the exciting laser line used in the SERS measurement (785 nm) falls within the SPR absorption peak.

To test the PLD Au substrates in vapor phase, 2 ppm concentration of 2NPT was created in the chamber (from drops of methanol solution of 2NPT) without saturating the atmosphere of the chamber with methanol. Also, complete evaporation of 2NPT was assured before carrying out the SERS measurements. As can be seen in Fig. 9, a clean spectrum of 2NPT can be obtained also from the vapor phase.

As in the case of the optical fiber sensor, the absence of the SH stretching peak (2567 cm^{-1}) reveals the formation of the SERS active sulfur-metal complex as a consequence of chemisorption of 2NPT from the vapor phase.

3.5. Time dependent behavior of the PLD Au substrates

Similar to the previous case (fiber-optic SERS sensor), we carried out time-dependent measurements on the PLD Au substrate, in order to evaluate the absorption kinetics and to determine the responsiveness and the sensibility of this SERS based sensor. The substrate was exposed to the 2NPT vapor in a flask maintained in a bath at 45 °C (to help quickly stabilize the diffusion processes within the flask, because of the required *ex-situ* setup). At different time interval the substrate was extracted from the flask and measurement carried out within few minutes.

The kinetics observed in the case of the PLD samples is reported in Fig. 10a.

Raman measurements were carried out with a micro-Raman apparatus; a reference mark was made on the surface to guarantee that the acquisition was performed at the same positions on the substrate surface, at know distances from the mark. The first spectrum was acquired after 30 s of exposure time to 2NPT vapors. The duration of the exposure time was from 30 s to 45 min with smaller intervals at early times.

From Figs. 9 and 10a, all the relevant peaks of 2NPT on PLD Au substrate can be observed. Intense peaks due to ring stretching modes are evident at 1382, 1451 and 1622 cm^{-1}, the peak at 1066 cm^{-1} is attributed to CH bending mode. Less intense, but still

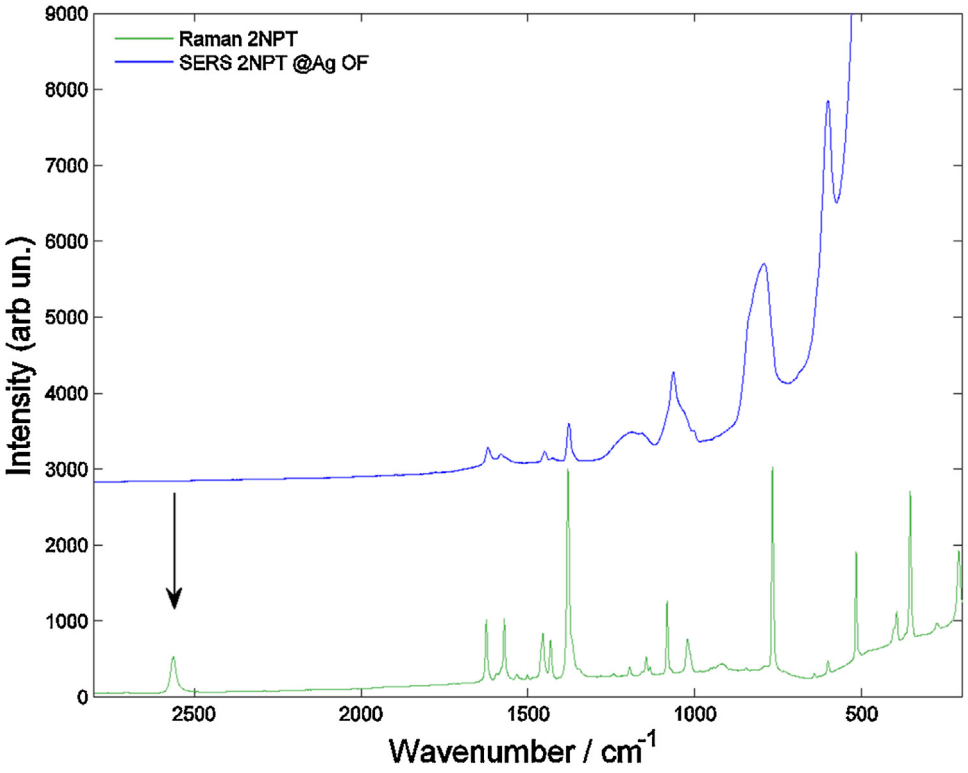

Fig. 5. Comparison between the normal FT-Raman spectrum of 2NPT and the SERS spectrum of 2NPT collected with the fiber optic sensor. Normal Raman and SERS spectra were acquired using respectively the 1064 nm and the 785 nm excitation wavelength. The arrow indicates the disappearance of the SH stretching line in the SERS spectrum, due to the formation of S-Ag bonds.

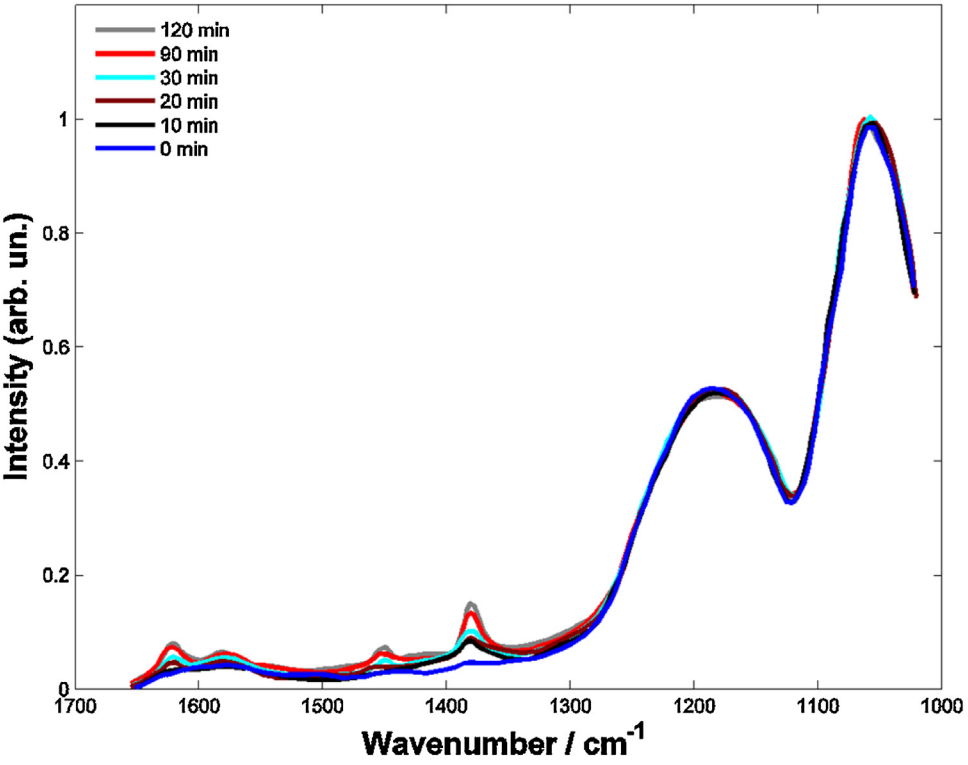

Fig. 6. Time-dependent measurement of the SERS spectra of 2NPT collected by the fiber optic sensor (785 nm excitation; exposure time of the sensor to 2NPT vapors from 10 min up to 120 min).

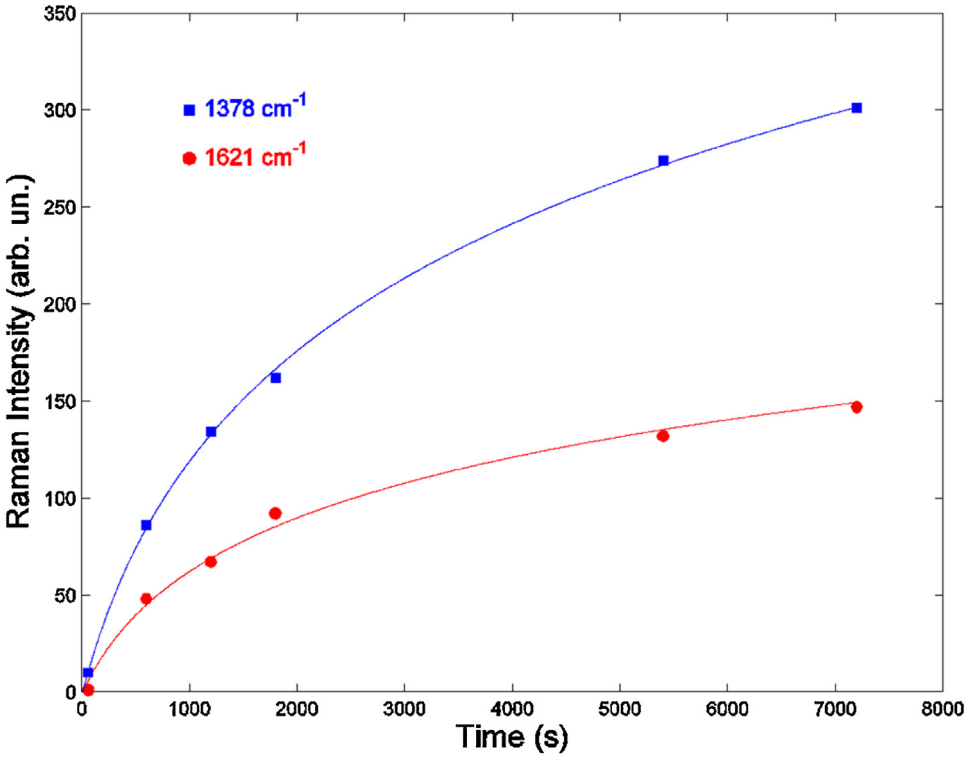

Fig. 7. Time-dependent measurement of the SERS spectra of 2NPT collected by the fiber optic sensor (785 nm excitation; exposure time of the sensor to 2NPT vapors from 10 min up to 120 min).

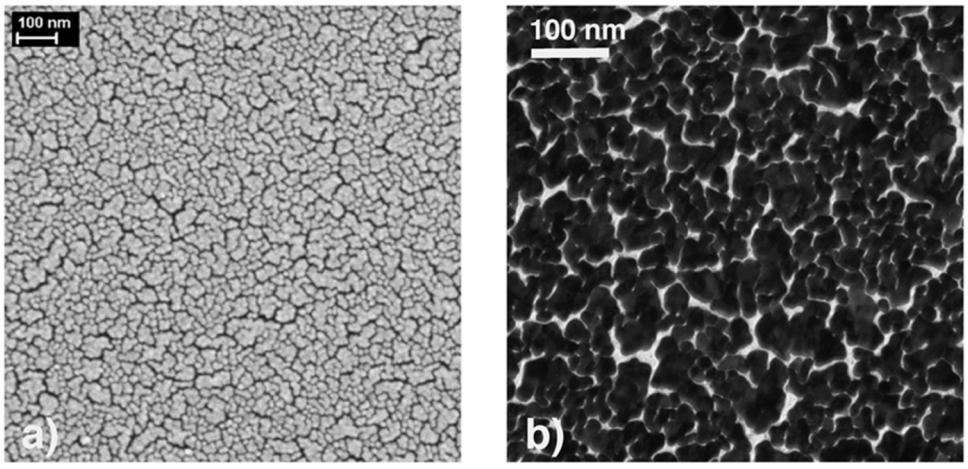

Fig. 8. (a) SEM and (b) TEM images of the surface of the PLD Au sample.

clearly visible, peaks are due to ring deformation modes at 518, 600, 640, 770 cm^{-1} and to ring stretching vibrations at 1431, 1452, 1569 and 1584 cm^{-1}. The feature at 846 cm^{-1} is due to CH twist mode and weaker peaks at 1156, 1146, 1024 and 1016 cm^{-1} are attributed to CH bending. For the first spectrum at 30 s, one is able to appreciate the background response of the substrate, but hints of the strongest peaks of 2NPT are still clearly visible pointing out for fast adsorption kinetics.

As it has been done for the fiber optic measurements, we followed, as function of time, the SERS peak intensity of the two most intense peaks (marked by asterisk in Fig. 10a; CC ring stretching at 1378 cm^{-1} and CH bending at 1066 cm^{-1}). The trend of the peak intensity *vs.* time is reported in Fig. 10b. Squares and stars refer to the measurements performed at two different positions. Peak intensities were normalized with respect to a mean of the values in the saturation region for all the different positions and their peak values. As can be seen the intensity of the 2NPT peaks grows with time until a saturation value is reached after about 250–300 s. Essentially the same behavior observed for the adsorption kinetics on the optical fiber, but it is worth noticing that the response of the planar PLD substrates is much faster.

The data were fitted using the Elovich model. The fit was limited to data points in the initial time of exposure just before the saturation plateau that, owing to the very fast kinetics adsorption occurred 4 min after the exposure of the substrate to 2NPT vapor. In the inset of Fig. 11, the semi-logarithm plot highlights how the Elovich model well describe the fast adsorption kinetics in this case also.

From the point of view of application as a sensor, a trend determined by adsorption kinetics has two great advantages: a) the

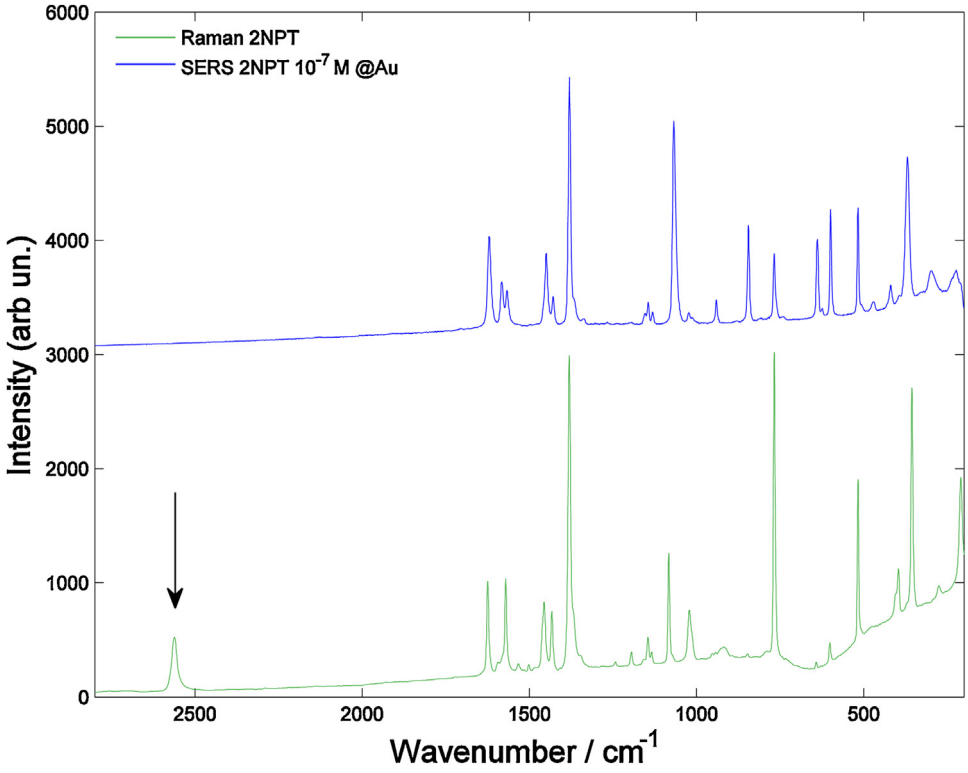

Fig. 9. SERS spectrum of 2NPT obtained in vapor phase at 2 ppm concentration with PLD Au substrate (785 nm excitation). This is compared with the normal Raman spectrum of 2NPT (1064 nm excitation). The arrow indicates the disappearance of the SH stretching line in the SERS spectrum, due to the formation of S-Au bonds.

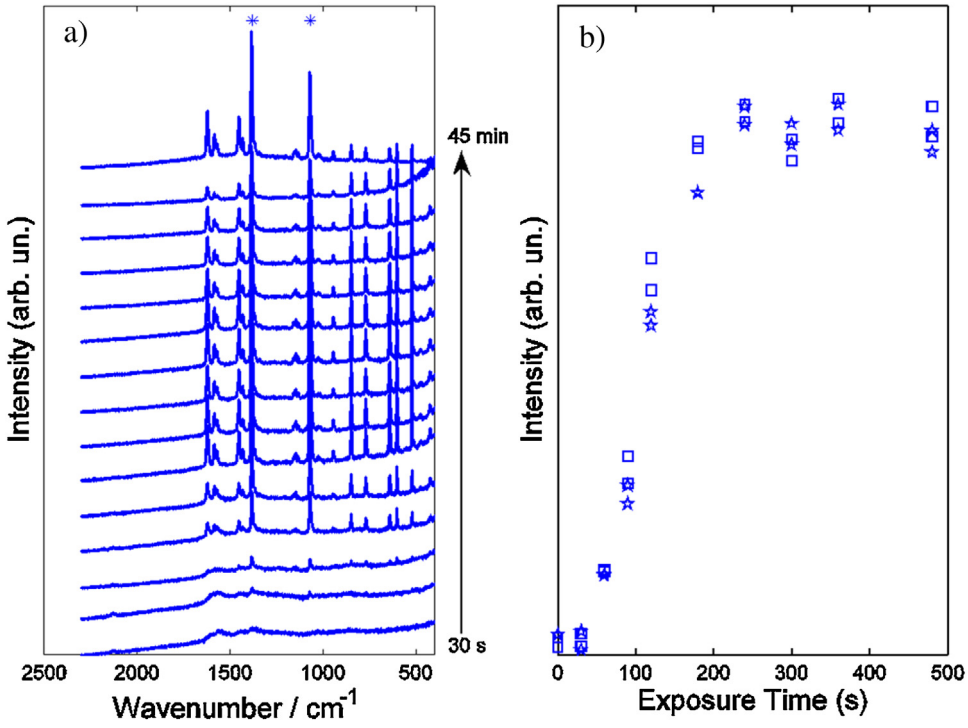

Fig. 10. (a) Time-dependent measurements of the SERS spectra of 2NPT adsorbed on the PLD Au substrate: (785 nm excitation wavelength; exposure time starting from 30 s up to 45 min); (b) Intensity of the two most intense SERS peaks (marked by asterisk, CC ring stretching at 1378 cm^{-1} and CH bending at 1066 cm^{-1}) *vs.* exposure time. Squares and stars refer to Spot A and Spot B positions respectively on the substrate where spectra were acquired.

large increase of the signal in the first minute represents a fast response and b) the possibility to use the same SERS sensor for measuring in the environment the integrated chronic exposure to a dangerous thiol substance (even at very low concentrations) like a dosimeter. Indeed, the signal intensity (on a logarithmic scale) is proportional to the time of exposure to harmful substances and, like every adsorption kinetics, the slope of the curve is related to the concentration of the analyte. In other words, the higher is the con-

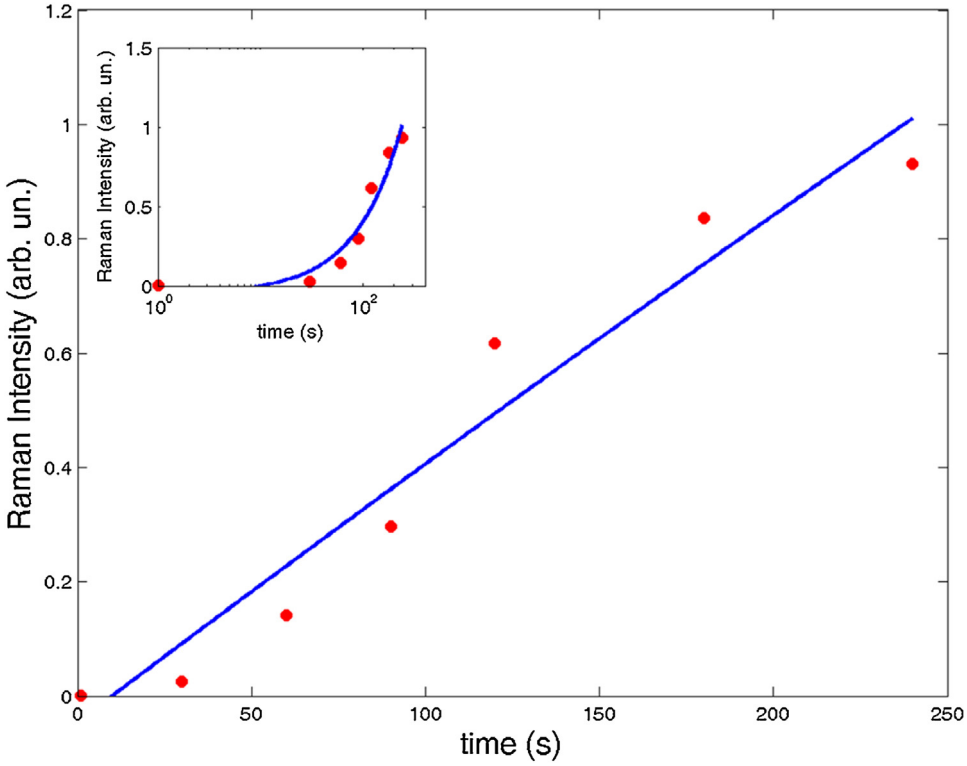

Fig. 11. Fit of the time dependence of the SERS peak intensity (mean of the values shown in Fig. 10b) for the PLD Au sensor. Inset illustrates the same curve in a semi-log plot since the adsorption kinetics follows Eq. (2).

centration of the harmful agent in the environment, the more rapid increase will be observed in the SERS signal intensity. A straightforward dose threshold setup can be made where the threshold refers to the measured SERS signal intensity (at a given time after deployment of the dosimeter). This threshold will be reached after a long time if the concentration of the harmful substance is low or vice versa.

4. Conclusions

The data presented in this work shows the good potential of two different SERS probes for the detection of volatile thiols. The fiber optic probe has the advantage of being prone to in-situ operation, possibly remote and in hazardous environments. The PLD SERS probe has comparable performance and can be used as environmental dosimeter.

We have characterized the time response of both sensors when exposed to a controlled atmosphere of 2NPT. The adsorption kinetics directly influences the rise of the SERS signal with time which can be fitted with a model of adsorption used in describing solid-gas interfaces (Elovich). The time response of the probes is concentration-dependent and can be considered adequate for online monitoring and applications as a dosimeter. Interestingly, when operated as dosimeter, the accumulation of thiols on the nanostructured surfaces allows detection of even trace concentrations of thiols over long exposure times. For instance, the fiber optic probe can detect a minimum of 0.1 ppb of 2NPT over 10 min of exposure, but lower concentrations could be detected with longer exposure times. This property may be particularly useful in scenarios where the chronic exposure to thiols is of concern.

Finally, by means of DFT calculations, we have analyzed in details the spectroscopic signals of 2NPT including the interaction with Ag and Au at the nearest neighbor level. This allowed the detailed assignment of the observed SERS signals. The results presented in this work pave the way for the possible use of SERS probes in industrial environments commonly exposed to thiols (e.g., oil industry).

Acknowledgements

This work was partly funded by Polisocial Award 2014, Project "Controllare l'epilessia nei Paesi in via di sviluppo" (Controlling epilepsy in Developing Countries).

Appendix A. Supplementary data

Supplementary data associated with this article can be found, in the online version, at http://dx.doi.org/10.1016/j.snb.2016.06.143.

References

[1] M. Moskovits, Surface-enhanced spectroscopy, Rev. Mod. Phys. 57 (1985) 783–826.
[2] K. Kneipp, H. Kneipp, J. Kneipp, Surface-enhanced Raman scattering in local optical fields of silver and gold nanoaggregates-from single-molecule Raman spectroscopy to ultrasensitive probing in live cells, Acc. Chem. Res. 39 (2006) 443–450.
[3] K. Kim, J.W. Lee, K.S. Shin, Detection of a few of biogenic volatile organic compounds by means of Raman scattering of isocyanide-adsorbed gold nanostructures, Spectrochim. Acta A 100 (2013) 15–20.
[4] J. Noh, E. Ito, M. Hara, Self-assembled monolayers of benzenethiol and benzenemethanethiol on Au(1 1 1): influence of an alkyl spacer on the structure and thermal desorption behavior, J. Colloid Interface Sci. 342 (2010) 513–517.
[5] C.J. Lee, H.J. Kim, M.R. Karim, M.S. Lee, Synthesis and characterization of silver/thiophene nanocomposites by UV-irradiation method, Mater. Lett. 61 (2007) 2675–2678.
[6] U.K. Sarkar, A pH-dependent SERS study of thiophene-2-carboxylic acid adsorbed on Ag-sols, Chem. Phys. Lett. 374 (2003) 341–347.
[7] M. Nishioka, Aromatic sulfur compounds other than condensed thiophenes in fossil fuels: enrichment and identification, Energy Fuels 2 (1988) 214–219.
[8] M. Li, T.G. Wang, B.R.T. Simoneit, S. Shi, L. Zhang, F. Yang, Qualitative and quantitative analysis of dibenzothiophene, its methylated homologues, and

benzonaphthothiophenes in crude oils coal, and sediment extracts, J. Chromatogr. A 1233 (2012) 126–136.
[9] S.G. Mössner, S.A. Wise, Determination of polycyclic aromatic sulfur heterocycles in fossil fuel-related samples, Anal. Chem. 71 (1999) 58–69.
[10] N.E. Moustafa, J.T. Andersson, Analysis of polycyclic aromatic sulfur heterocycles in Egyptian petroleum condensate and volatile oils by gas chromatography with atomic emission detection, Fuel Process. Technol. 92 (2011) 547–555.
[11] J.P. Mathews, A.C.T. Van Duin, A.L. Chaffee, The utility of coal molecular models, Fuel Process. Technol. 92 (2011) 718–728.
[12] J.P. Mathews, A.L. Chaffee, The molecular representations of coal—a review, Fuel 96 (2012) 1–14.
[13] R.A. Alvarez-Puebla, D.S. Dos Santos Jr., R.F. Aroca, Surface-enhanced Raman scattering for ultrasensitive chemical analysis of 1 and 2-naphthalenethiols, Analyst 129 (2004) 1251–1256.
[14] A. Pesapane, A. Lucotti, G. Zerbi, Fiber-optic SERS sensor with optimized geometry: testing and optimization, J. Raman Spectrosc. 41 (2010) 256–267.
[15] N.R. Agarwal, F. Neri, S. Trusso, A. Lucotti, P.M. Ossi, Au nanoparticle arrays produced by pulsed laser deposition for surface enhanced Raman spectroscopy, Appl. Surf. Sci. 258 (2012) 9148–9152.
[16] N.R. Agarwal, E. Fazio, F. Neri, S. Trusso, C. Castiglioni, A. Lucotti, N. Santo, P.M. Ossi, Ag and Au nanoparticles for SERS substrates produced by pulsed laser ablation, Cryst. Res. Technol. 46 (2011) 836–840.
[17] C. Zanchi, A. Lucotti, M. Tommasini, S. Trusso, U. De Grazia, E. Ciusani, P.M. Ossi, Au nanoparticle-based sensor substrates for apomorphine detection in plasma, Beilstein J. Nanotechnol. 6 (2015) 2224–2232.
[18] P.C. Lee, D.J. Meisel, Adsorption and surface-enhanced Raman of dyes on silver and gold sols, J. Phys. Chem. 86 (1982) 3391–3395.
[19] A. Lucotti, G. Zerbi, Fiber-optic SERS sensor with optimized geometry, Sens. Actuators B 121 (2007) 356–364.
[20] A. Lucotti, M. Casella, M. Tommasini, Book on Enhanced Spectroscopy Surface-Enhanced Multipurpose Nanosensing with Microneedle-Shaped Fiber Optics, 2015, pp. 283–305 (Chapter 8).
[21] D. Figgen, G. Rauhut, M. Dolg, H. Stoll, Energy-consistent pseudopotentials for group 11 and 12 atoms: adjustment to multi-configuration Dirac–Hartree–Fock data, Chem. Phys. 311 (2005) 227–244.
[22] K.A. Peterson, C. Puzzarini, Systematically convergent basis sets for transition metals. II. Pseudopotential-based correlation consistent basis sets for the group 11 (Cu, Ag Au) and 12 (Zn, Cd, Hg) elements, Theor. Chem. Acc. 114 (2005) 283–296.
[23] The Gaussian09 rev. A.02 computer program [Gaussian 09, Revision A.02] M. J. Frisch, G.W., Trucks, H.B., Schlegel, G.E., Scuseria, M.A., Robb, J.R., Cheeseman, G., Scalmani, V., Barone, B., Mennucci, G.A., Petersson, H., Nakatsuji, M., Caricato, X., Li, H.P., Hratchian, A.F., Izmaylov, J., Bloino, G., Zheng, J.L., Sonnenberg, M., Hada, M., Ehara, K., Toyota, R., Fukuda, J., Hasegawa, M., Ishida, T., Nakajima, Y., Honda, O., Kitao, H., Nakai, T., Vreven, J.A., Montgomery, Jr., J.E. Peralta, F., Ogliaro, M., Bearpark, J.J., Heyd, E., Brothers, K.N., Kudin, V.N., Staroverov, R., Kobayashi, J., Normand, K., Raghavachari, A., Rendell, J.C., Burant, S.S., Iyengar, J., Tomasi, M., Cossi, N., Rega, J.M., Millam, M., Klene, J.E., Knox, J.B., Cross, V., Bakken, C., Adamo, J., Jaramillo, R., Gomperts, R.E., Stratmann, O., Yazyev, A.J., Austin, R., Cammi, C., Pomelli, J.W., Ochterski, R.L., Martin, K., Morokuma, V.G., Zakrzewski, G.A., Voth, P., Salvador, J.J., Dannenberg, S., Dapprich, A.D., Daniels, Ö., Farkas, J.B., Foresman, J.V., Ortiz, J. Cioslowski, and D. J. Fox, Gaussian, Inc., Wallingford CT, 2009.
[24] C. Johannessen, E.W. Blanch, C. Villani, S. Abbate, G. Longhi, N.R. Agarwal, M. Tommasini, D.A. Lightner, Raman and ROA spectra of (−)-and (+)-2-Br-Hexahelicene: experimental and DFT studies of a π-conjugated chiral system, J. Phys. Chem. B 117 (2013) 2221–2230.
[25] M.J.D. Low, Kinetics of chemisorption of gases on solids, Chem. Rev. 60 (1960) 267–312.
[26] C. D'Andrea, F. Neri, P.M. Ossi, N. Santo, S. Trusso, The controlled pulsed laser deposition of Ag nanoparticle arrays for surface enhanced Raman scattering, Nanotechnology 20 (2009) 245606.
[27] M.C. Spadaro, E. Fazio, F. Neri, S. Trusso, P.M. Ossi, On the role of the ablated mass on the propagation of a laser-generated plasma in an ambient gas, EPL 109 (2015) 25002.
[28] N.R. Agarwal, F. Neri, S. Trusso, P.M. Ossi, Growth analysis of pulsed laser ablated films, Plasmonics 8 (2013) 1707.
[29] N. Micali, F. Neri, P.M. Ossi, S. Trusso, Light scattering enhancement in nanostructured silver film composites, J. Phys. Chem. C 117 (2013) 3497.

Biographies

Nisha Rani Agarwal is a post-doctoral researcher at the Molecular microscopy group at Chalmers University of technology. She received her PhD in Materials Engineering in 2013 at Politecnico di Milano for the study of controlled synthesis of noble metal SERS substrates by pulsed laser deposition for application as biosensors. She pursued her first post-doc at Istituto Italiano di tecnologia, Genova for setting up Stimulated Raman Scattering microscopy. She continued in the field of non-linear microscopy at Chalmers specializing in techniques as CARS, SHG, AFM, SNOM and TERS for study of Alzheimers disease, Colo-rectal cancer and plasmonics.

Andrea Lucotti, PhD in Materials Engineering, Politecnico di Milano, 2005, is a researcher at the Department of Chemistry, Materials and Chemical Engineering "Giulio Natta" (Politecnico di Milano). In 2014 he got the habilitation as Associate Professor according to the Italian National Scientific Habilitation Procedure (ASN 2012), Scientific-disciplinary Sector "Materials Science and Technology". His research interests include science of organic functional materials, polymers, photochromic materials, nanostructured carbon materials and carbon nanowires, nanostructured metals and metal nanoparticles, Raman spectroscopy, SERS (Surface Enhanced Raman Spectroscopy), fiber-optic SERS sensors, infrared spectroscopy, UV-VIS-NIR absorption spectroscopy and spectrofluorimetry.

Matteo Tommasini was born in 1972 in Desenzano del Garda (Brescia, Italy). At Politecnico di Milano (Italy), he graduated in Nuclear Engineering in 1998 and he obtained his PhD in Materials Engineering in 2002 under the guidance of Prof. G. Zerbi and Prof. C. Castiglioni. He is associate professor in Materials Science and Technology at Politecnico di Milano. His research interest focuses on the applications of Vibrational Spectroscopy and Quantum Chemistry to Materials Science and Biotechnology.

Fortunato Neri is a Full Professor of Experimental Physics in University of Messina, since 2005. His expertise is mainly in experimental studies and technological applications developments in the solid state physics field, mostly devoted to thin films deposition techniques, nanostructured materials synthesis and spectroscopic diagnostic investigations. Co-author of over 120 publications in international scientific journals, he is manager of some research laboratories: Microanalysis Laboratory (X-ray Photoelectron Spectroscopy & Imaging, Auger e Reflection Energy Loss Spectroscopy); Spectroscopic Techniques Laboratory (Raman Microscopy & Imaging and conventional optical spectroscopies); Nanotechnology Laboratory (Laser Ablation in Liquids).

Sebastiano Trusso received an MSc in Physics at the University of Messina. He is a researcher at the IPCF-CNR in Messina. His main research is focused on the growth of noble metal nanoparticles by pulsed laser ablation for surface enhanced Raman scattering applications. Other research interests are semiconductor and metal oxide thin film deposition by pulsed laser ablation and plasma spectroscopy of laser generated plasmas. He is co-author of more than 100 publications in international scientific journals.

Paolo M. Ossi, PhD in Solid State Physics, University of Parma, 1979, is associate professor in Physics of Matter at Politecnico di Milano, Winter sport and bio nanodiagnostics – WIBIDI Lab. Research interests in modeling laser-generated plasma dynamics in dense fluids, synthesis of nanoparticles in plasmas and their application as biosensors, plasma-surface interactions (metals, ceramics), formation of metastable phases under energetic particle/photon bombardment, synthesis of snow and its properties under irradiation.